Appendix D: Oceanic heat flux

In order to estimate the oceanic heat flux q_w required to sustain the basal melt rates a_b ($m\,s^{-1}$) derived in this study, we separate the heat flux q_w into two components: the heat flux to melt the ice (q_m) and the heat flux into the glacier interior (q_i) that is required for heating the ice by ΔT to the pressure melting point:

$$q_w = \underbrace{\rho_i\, a_b\, L}_{q_m} + \underbrace{\rho_i\, c_i(T)\, a_b\, \Delta T}_{q_i}. \quad \text{(D1)}$$

The heat fluxes depend on the density of the ice, $\rho_i = 917\,kg\,m^{-3}$; the latent heat of fusion, $L = 334\,000\,J\,kg^{-1}$; and the specific heat capacity for ice, $c_i(T) = 146.3 + 7.253 \cdot T\,[K]\,J\,kg^{-1}\,K^{-1}$ with the temperature T in kelvin CE10 (Ritz, 1987).

To obtain an estimate of the heat flux that the ocean can provide, we follow the approach implemented in the Finite Element Sea ice–Ocean Model (FESOM; Timmermann et al., 2012). Here, a three-equation system is used that determines the temperature and salinity of a thin boundary layer along the ice-shelf base from its heat and freshwater exchange with the ice and the ambient ocean (Hellmer and Olbers, 1989; Holland and Jenkins, 1999). Besides the ocean temperature, the heat flux into this boundary layer is determined by the flow velocity in the ambient ocean, as the latter determines the friction and, thus, defines the turbulent fluxes of heat and salt (Jenkins and Doake, 1991).

Appendix E: Hydrostatic imbalance near the grounding line

Basal melt rates can be estimated from surface elevation changes once hydrostatic flotation of the ice can be assumed. In the hinge zone, downstream of the upper flexure limit, bending dominates the vertical motion; hence, one has to assess the validity of the assumption of hydrostatic flotation. To validate this assumption near the grounding line of 79NG, we analyzed the hydrostatic imbalance by calculating the vertical mean ice density $\bar{\rho}_i$ assuming that the ice is in hydrostatic equilibrium. Here, we used the ice thickness H from the UWB airborne radar data and surface elevation h from the airborne laser scanner. Both data sets were obtained from the same flights in July 2021. The averaged vertical ice density can be calculated as follows:

$$\bar{\rho}_i = \rho_{oc} \frac{H - h}{H}, \quad \text{(E1)}$$

where $\rho_{oc} = 1028\,kg\,m^{-3}$ is the density of the ocean. We defined a plausible range of vertical mean ice densities of between 900 and $917\,kg\,m^{-3}$. The results show high variability in the ice density in the hinge zone and also downstream where the ice is freely floating. Densities below $900\,kg\,m^{-3}$

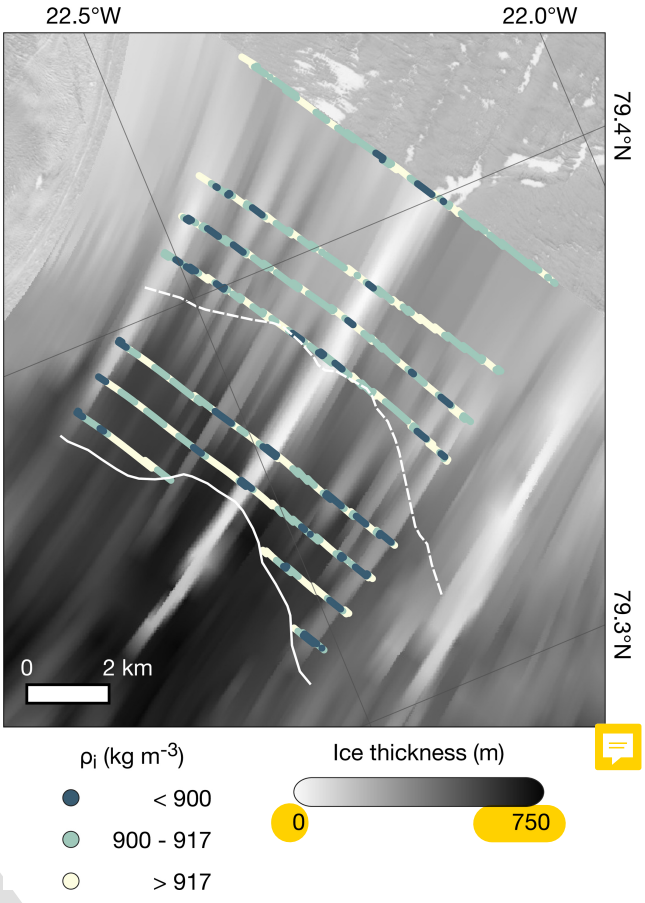

Figure E1. Computed ice density (dots) assuming the ice is in hydrostatic equilibrium based on ice thickness from UWB data (background) and surface elevation from airborne laser scanner data from the same flights in 2021. The solid white line shows the upper flexure limit (grounding line) and the dashed white line shows the lower flexure limit. CE11

(dark blue dots in Fig. E1) are reached above basal channels where the ice is thin, especially near the grounding line. This indicates that the ice above the channels near the grounding line is not in hydrostatic equilibrium, in contrast with the ice above smaller channels downstream of the hinge zone. Here, the ice density is widely above $900\,kg\,m^{-3}$, except above the large central channel. This result is consistent with the findings of Chartrand and Howat (2023). Near the grounding line, ice densities outside of the channels are above $900\,kg\,m^{-3}$ and widely also above $917\,kg\,m^{-3}$. The results show that hydrostatic equilibrium cannot be assumed in the hinge zone nor above the basal channels even further downstream, as one would expect from the viscoelastic material behavior of ice. Thus, in these areas, surface elevation changes cannot be used for the calculation of ice thickness changes.